Deployable Mirror for Enhanced Imagery Suitable for Small Satellite Applications

James A. Champagne, Blake G. Crowther, Trent T. Newswander
Utah State University Research Foundation Space Dynamics Laboratory
1695 North Research Park Way, North Logan, Utah 84341; 435-713-3428
James.Champagne@sdl.usu.edu

ABSTRACT

High spatial resolution imagery and large apertures go hand in hand but small satellite volume constraints place a direct limit on monolithic aperture mirror systems. Deployable optical systems hold promise of overcoming aperture size constraints and greatly enhancing small satellite imaging capabilities. The Space Dynamics Laboratory (SDL) is currently researching deployable optics suitable for small spacecraft and has developed a passively aligned deployable mirror. The team recently built a proof-of-principle mirror and a single parabolic mirror segment or "petal" measured for deployment repeatability. They measured elevation (tilt) and azimuth (tip) angular alignment repeatability to be 0.6 arcseconds or 2.9 μrad (1 sigma) in each axis after a ten deployment sequence. The SDL team used optical modeling to study the effects of these alignment errors on a multiple petal parabolic primary mirror part of a Cassegrain imaging system. The model indicates that excellent image quality is possible in the short wave infrared (SWIR) to long wave infrared (LWIR) bands. Work continues on a four segment deployable primary mirror with an aperture diameter of 152 mm. The goal is to fabricate the mirror segments and demonstrate repeatable interferometric wavefront error measurements.

INTRODUCTION ON DEPLOYABLE OPTICS

Two well-known fundamental scientific principles illustrate the importance of telescope aperture. First, the angular spread of the irradiance blur due to diffraction is inversely proportional to the extent of the entrance or exit pupils. This can be seen in the equations for the angular distance between the first dark zones in the Fraunhofer diffraction region in Equation 1 for a square aperture and Equation 2 for a circular aperture.[1]

$$\beta = \left(\frac{2\lambda}{a} \right) \quad \textbf{(1)}$$

$$\beta = \left(\frac{2.44\lambda}{a} \right) \quad \textbf{(2)}$$

These equations use β for the full angular blur, λ for the wavelength, and a for linear side-to-side distance in the case of a rectangular pupil and diameter in the case of a circular pupil. The power inside the central blur is inversely proportional to the length times the width of the pupil or the pupil diameter squared.[1]

The second principle concerns the power or photon flux collected by the telescope and subsequently relayed to the detector. The power collected is proportional to the area of the aperture in the case of a point source as shown in Equation 3, where Φ represents the flux collected, E is the irradiance at the aperture of the sensor due to emission from the point source, and A_{EP} is the area of the entrance pupil.[2]

$$\Phi = EA_{EP} \quad \textbf{(3)}$$

In the case of an extended area source, the power received is usually written as shown in Equation 4, where Φ represents the power or photon rate collected, L is the extended source radiance, and F is the focal ratio or F/# (focal length divided by the entrance pupil diameter) of the optical system. Note that in this case, the flux is proportional to the reciprocal of the F/# squared.[2]

$$\Phi = \frac{L\pi}{4F^2} \quad \textbf{(4)}$$

In Equation 3, the area is just the length times the width of the pupil or π times the diameter squared over four. In Equation 4, substitution for the F/# will place the square of the entrance pupil diameter in the numerator and the square of the focal length in the denominator. Thus, both of these equations for received signal demonstrate that the received power is a function of the square of the dimension of the entrance pupil.

The above simple equations show why the telescope dimension is important for both the resolution and the signal collection capability. The problem is that there are often envelope and mass requirements that ultimately restrict the size of the telescope. The obvious

solution to this situation is to develop a deployable telescope that can be folded to enable accommodation within the requirements but when unfolded, is large enough to deliver the required resolution and signal. While the solution is simple in concept, it has proven to be a difficult implementation challenge.[3]

The SDL team has designed a patent-pending Deployable Petal Telescope (DPT) that is both simple and robust. The DPT offers a means to achieve higher resolution imaging and an improved Signal-to-Noise Ratio (SNR) in a smaller envelope. The increase in surface area and aperture extent using the DPT is shown in Table 1.

Table 1: Monolithic vs. DPT Mirror

Mirror Type	Aperture Area (cm²)	Aperture Diameter (cm)
Monolithic Mirror	48.4	8.1
DPT Mirror	80.0	15.2
% Increase	65%	90%

DPT uses a deployable multi-petal primary mirror and deployable monolithic secondary mirror to create a larger telescope than possible within a fixed volume constraint. It is built on modern precision fabrication techniques, which permits simple passive deployment and alignment mechanisms, resulting in lower costs than other actively aligned deployable telescopes. During the initial phase of research, the team focused their efforts on a single petal of a multi petal primary mirror designed for a Cassegrain optical imaging system. The key item in the DPT concept is the primary mirror as it must be aligned most precisely. The concept design uses four petals and facilitates compact packaging while still delivering good image quality.

Small Sat Platform Volume Accommodation

The DPT prototype was designed to stow within an 8.1 cm diameter tube, slightly smaller than the optic diameter constraint placed on a 1U payload volume. When fully deployed, the effective aperture diameter nearly doubles to 15.2 cm. A depiction of the volume utilization of the DPT in relation to an 8.1 cm diameter monolithic mirror is shown in Figure 1.

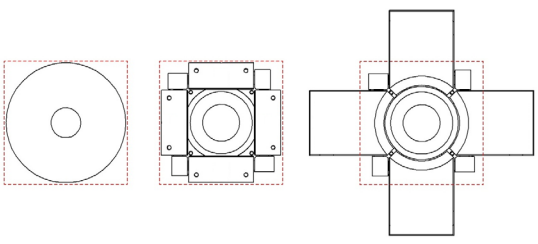

Figure 1: DPT Stowed Volume Utilization

Small Satellite Resolution Enhancement

Many factors contribute to the spatial resolution obtainable by a remote sensing system. These include the point spread function (PSF) of the optical system, the size and sampling of the detector system, relative object-sensor motion, the quality of the readout electronics, and the quality of the display medium. This paper addresses the first consideration, which is the effect of the sparse aperture on the final image quality.

It is well known that a cross shaped aperture, which is composed of two overlapping rectangular sections, produces a $Sinc^2$ irradiance pattern at the focal plane while a circular aperture produces an Airy function.[1] One effect of the DPT is to produce an asymmetric PSF with a tighter distribution in the directions of the DPT petals. The team estimated the effect of a 1U (~10 cm) aperture and that of a DPT capable of doubling this aperture by convolving the respective PSFs with a test image using Code V optical design software as shown in Figure 2. The top panel illustrates the standard image obtainable by an F/7 Ritchey-Chrétien telescope with a monolithic 1-U primary. The bottom panel shows the enhancement obtainable from a DPT that would double the linear dimensions of the primary mirror and entrance pupil. The improved detail of the bottom panel shows that the DPT produces substantially improved imagery.

Figure 2: Monolithic 1U Circular Primary Mirror Simulated Imagery (top panel) vs. a Doubled Aperture Linear Dimension DPT (bottom panel)

Optical Design

The DPT prototype telescope optical design consists of a two mirror Cassegrain telescope comprising a parabolic primary and hyperbolic secondary. This common optical configuration is well suited for deployable optics due to its rotational symmetry and separation between optical components, allowing the primary to be folded in a compact stowed position. Figure 3 and Figure 4 show the Cassegrain layout with a representation of a four segment primary. After reflecting from the parabolic primary mirror, the optical rays converge to a hyperbolic secondary mirror and are then reflected to a focus accessible behind the segmented primary mirror.

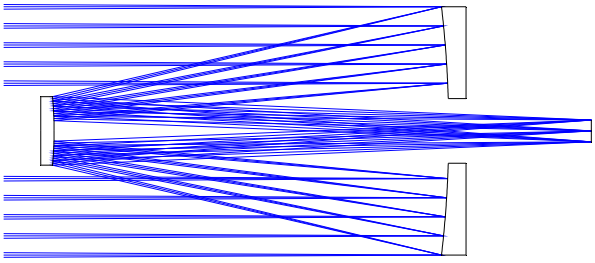

Figure 3: Cassegrain Optical Layout

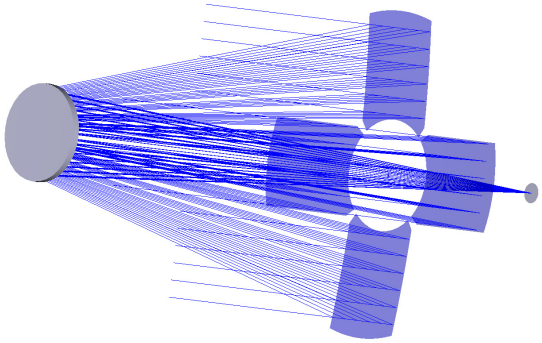

Figure 4: Cassegrain with Segmented Primary

The system focal length is 1067 mm and entrance pupil diameter is 153 mm, working at F/7. Even though this is a fairly slow optical system, the primary mirror is a fast component. As a stand-alone optic, the primary mirror would operate near F/2. This means that its alignment/positional and figure tolerances will be stringent, especially for the shorter visible wavelengths.

Mechanical Design

The mechanical design must transition a single optic petal from the stowed to deployed position and locate the optic accurately with respect to the other petals. Deployment involves the rotation of the petal from the stowed position to the fully deployed imaging configuration. Figure 5 and Figure 6 show the single petal hardware when stowed and fully deployed.

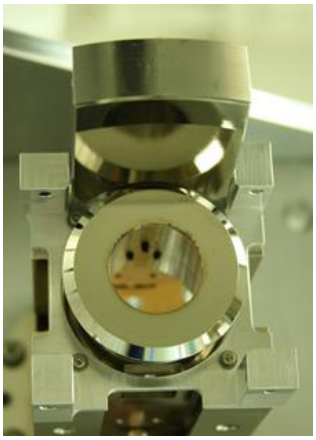

Figure 5: Stowed Configuration

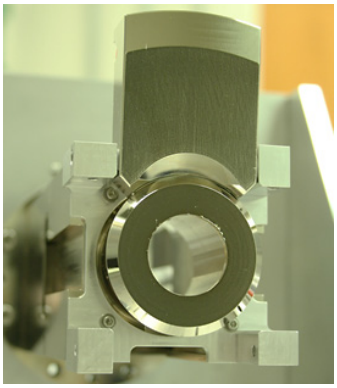

Figure 6: Deployed Configuration

The mechanical force required to deploy the petal is provided by a spring engine. Force from the spring engine is transferred to the petal via a tensioned cable. The petal is held in the stowed position by a non-explosive actuator (NEA) such as a pin-puller. Once the petal is released, the cable tension rotates the petal about a guide hinge to the deployed position. Final positioning of the petal is commanded by a semi-kinematic interface between the petal and the base support. Mechanical spring force retains the petal in the deployed position.

No electrical components are required for the deployment and final positioning. This passive alignment system eliminates the cost, complexity, and mass associated with active alignment. Only a single electrical signal is required for the NEA to initiate telescope deployment.

Single Deployable Mirror Proof of Concept Test

The single deployable mirror proof of concept test provides repeatability of optical positioning data for the deployment of a single mirror petal. Successful repeatability provides a proof of the concept that multiple petals can be aligned on the ground, stowed, and later deployed with high optical precision.

For the single petal test, the paraboloid portion of the optic was not used but rather a flat reflective section near the edge of the petal, as can be seen in the Figure 5 and Figure 6. The single petal alignment test was performed using an electronic autocollimator obtaining a return from the reflective flat as shown in Figure 7.

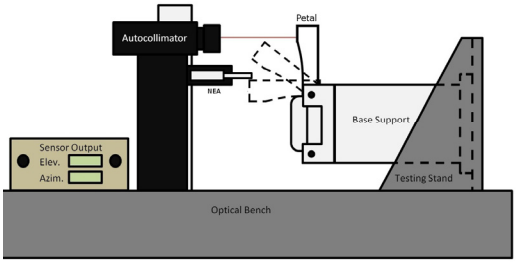

Figure 7: Experimental Test Setup

The electronic autocollimator measures the angular alignment of two axes simultaneously, elevation and azimuth. The elevation axis corresponds with rotation about the x-axis and the azimuth corresponds with rotation about the y-axis as defined by the petal coordinate system shown in Figure 8.

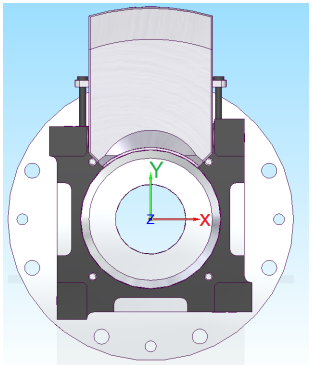

Figure 8: Petal Coordinate System

The petal is held in the stowed position with a NEA. As the NEA is activated, the petal is released and rotates about the hinge until fully engaged with the positioning components. A period of time (10-15 minutes) is allowed to pass before an angular measurement is taken. This ensures the petal has fully deployed to its final seating position. After the measurement, the petal is re-stowed and the deployment sequence is repeated.

Proof of Concept Results

SDL performed repeatability tests with the gravity vector along -Y, +X, and +Y as defined by the coordinate system in Figure 8. These configurations were obtained by simply rotating the petal assembly 90 and 180 degrees on its test fixture. Results of ten consecutive deployments for each case are presented in Table 2.

Table 2: Proof of Concept Repeatability Test Results

Gravity Vector Orientation	- Y	+ X	+ Y
Average Azimuth Error [arcsec]	-0.7	1.2	0.1
Standard Deviation Azimuth Error [arcsec]	0.5	0.6	0.3
Average Elevation Error [arcsec]	0.1	0.6	-0.6
Standard Deviation Elevation Error [arcsec]	0.6	0.3	0.4

After the first deployment, the electronic autocollimator was zeroed and the rest of the deployments were measured relative to this initial deployment position. All gravity vector orientations produced a repeatability standard deviation less than 0.6 arcseconds in both the azimuth and elevation axes. Conversion of this angular alignment error to petal outer edge linear position error results in 170 nm for the elevation axis and 52 nm for the azimuth axis.

OPTICAL MODEL ALIGNMENT SENSITIVITY ANALYSIS

The team created an optical model of a deployable Cassegrain telescope using ZEMAX optical design and modeling software to simulate alignment errors. With this model, it is possible to predict how well the system will perform at different wavelengths. The proof of concept test measured the azimuth and elevation angular alignment errors of a single petal within a four petal primary mirror system. The optical model was used to predict the performance of a Cassegrain system with a four petal primary mirror assuming the standard deviation angular alignment errors measured in the single petal experiment.

ZEMAX Non-Sequential Optical Model

ZEMAX has two modes of operation. The majority of optical designs are accomplished in the sequential mode where rays propagate from surface to surface in a predefined sequence. The non-sequential mode in ZEMAX can be used to model a grouping of 3-dimensional objects and their interactions with rays. There are no predefined paths in this mode and the positions of each optical element are defined independently of one another. The non-sequential model is required for alignment tolerance analysis of a segmented aperture, allowing individual mirror segments to be misaligned independent of the other segments. In the test case, a mixed-mode sequential/non-sequential model was used to model the segmented primary of the DPT. Rays enter and exit a non-sequential area where the petals are contained. Within this region, each petal can be misaligned independently of the other petals. Rays that reflect from the misaligned petals then propagate away from the non-sequential region and reflect from the secondary and then to the focal plane in a sequential manner.

Petal Alignment Sensitivity

Each petal has six degrees of freedom: XYZ translation and XYZ rotation. Each petal is capable of being misaligned in any one of these degrees of freedom. The optical model was used to determine image quality degradation as a single petal was misaligned in each degree of freedom with no focus compensation at the focal plane. Table 3 presents the alignment sensitivities.

Table 3: Single Petal Alignment Sensitivity Analysis

Parameter/Error	Sensitivity	Units
X-Translation/Decenter	12	nm RMS / µm
Y-Translation/Decenter	19	nm RMS / µm
Z-Translation/Piston	498	nm RMS / µm
X Rotation/Elevation	58	nm RMS / arcseconds
Y Rotation/Azimuth	45	nm RMS / arcseconds
Z Rotation/Clocking	1	nm RMS / arcseconds

For this sensitivity analysis, the degradation to the field averaged RMS wavefront error was calculated for a full field of view of 0.5°. The nominal field averaged RMS wavefront error of the Cassegrain system is 47 nm RMS.

The sensitivity analysis shows that Z-translation, or piston, is the most sensitive alignment parameter. The opto-mechanics were designed such that a single feature on the base mount controls piston of all four mirror segments simultaneously, eliminating the likelihood of a pure piston error. The next two most sensitive parameters are X Rotation and Y Rotation, which were measured experimentally in the single petal repeatability test. SDL expects these two alignment errors to contribute most to image quality degradation and the final image quality of the system. The petal is fairly insensitive to X Translation, Y Translation, and Z Rotation as the opto-mechanical design controls these errors very well.

Using the sensitivities for elevation and azimuth alignment errors for a single petal, an estimate of the RMS wavefront error degradation from four misaligned petals can be computed. For this computation, the team assumed a 0.6 arcsecond misalignment in the elevation and azimuth axis of each petal. Thus each petal contributes 35 nm RMS wavefront error due to the elevation misalignment and 27 nm RMS wavefront error due to the azimuth misalignment. Taking an RSS of the contributions from all four petals, the estimated wavefront error degradation is 88 nm RMS. Adding this to the nominal design residual, the team obtained a system wavefront error of 135 nm RMS. There will be other sources of error in the system such as optical figure, surface irregularity, secondary alignment, and sensor alignment. It is assumed that the tolerance budget for these errors will total 50% of the nominal RMS wavefront error or 24 nm RMS, giving a new system wavefront error of 160 nm RMS.

Based on the errors of this system, multiplying the system RMS wavefront error by a factor of 4 gives an estimate to the peak-to-valley wavefront error.[4] Thus the estimated peak-to-valley wavefront error is 640 nm. Assuming the quarter-wave criterion for diffraction limited performance, this peak-to-valley wavefront error will yield diffraction limited performance for wavelengths of 2.5 µm and above.

SWIR Monte Carlo Analysis

The ZEMAX optical model was also used to perform a Monte Carlo analysis in the SWIR and mid-wave infrared (MWIR) to supplement the previous wavefront error calculation. A normal statistical distribution was assumed with a ± 1.2 arcsecond tolerance range (2 sigma) for the elevation and azimuth alignment of each petal. The parameter of interest is the modulation transfer function (MTF), a measure of contrast or how well a system is able to reproduce spatial frequencies. The Nyquist cutoff frequency of a SWIR sensor with a pixel pitch $\Delta X = 15$ µm is calculated using Equation 5.[4]

$$f_N = \frac{1}{2\Delta X} = 33 \frac{cycles}{mm} \quad \textbf{(5)}$$

The maximum frequency of the MTF plots were set to this value and a polychromatic wavelength range from 1 – 3 µm was assumed, covering the SWIR. The nominal polychromatic MTF of the Cassegrain system is presented in Figure 9 for three field points over a 0.5° full field of view.

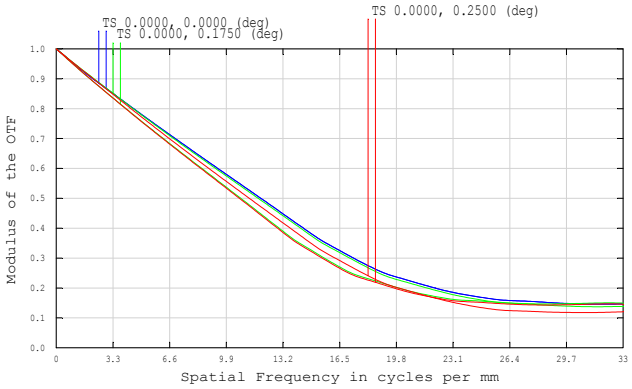

Figure 9: System Nominal SWIR MTF

The Monte Carlo simulation was run 100 times, perturbing all four petals in the elevation and azimuth axes. Figure 10, Figure 11, and Figure 12 give an overlay of all 100 runs in a single MTF plot with each plot showing a different field angle. For reference, the

diffraction limited MTF curve for this system is plotted in black within each figure. Statistics of the Monte Carlo simulation are presented in Table 4.

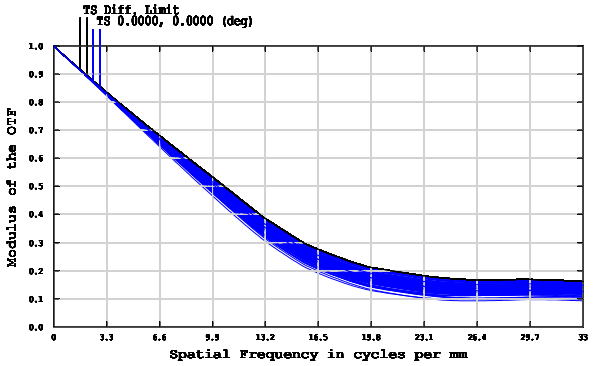

Figure 10: Monte Carlo Analysis On-Axis SWIR MTF

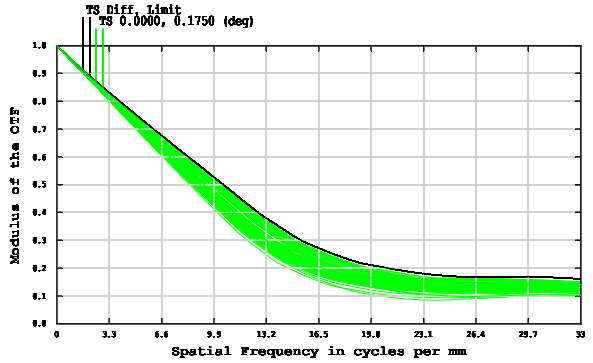

Figure 11: Monte Carlo Analysis 0.175° Field SWIR MTF

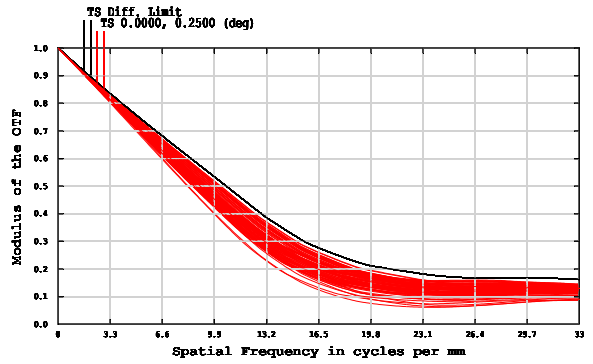

Figure 12: Monte Carlo Analysis 0.25° Field SWIR MTF

Table 4: SWIR 100 Trial Monte Carlo Statistics

Statistic	Wavefront Error
Nominal WFE	47 nm RMS
Best Trial	59 nm RMS
Worst Trial	313 nm RMS
Mean	167 nm RMS
Standard Deviation	51 nm RMS

The MTF plots give a worst case contrast loss of 50% and an average loss of 20% at mid-spatial frequencies. The statistics of the run produce a mean system wavefront error of 167 nm RMS with a standard deviation of 51 nm RMS. These plots and analysis show that the current DPT alignment performance is capable of average to excellent image quality in the SWIR.

MWIR Monte Carlo Analysis

The same Monte Carlo simulation was performed for MWIR wavelengths 3 – 5 µm. Figure 13 shows the nominal system MTF for this wavelength range. Figure 14, Figure 15, and Figure 16 show a similar Monte Carlo analysis at the MWIR wavelengths.

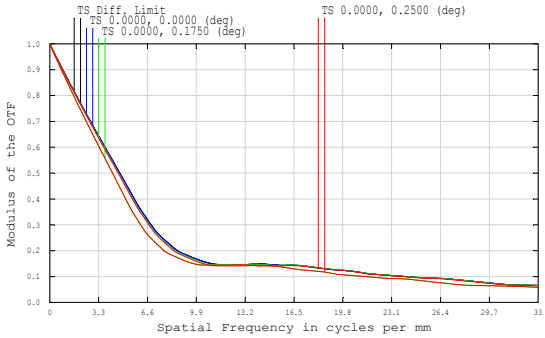

Figure 13: System Nominal MWIR MTF

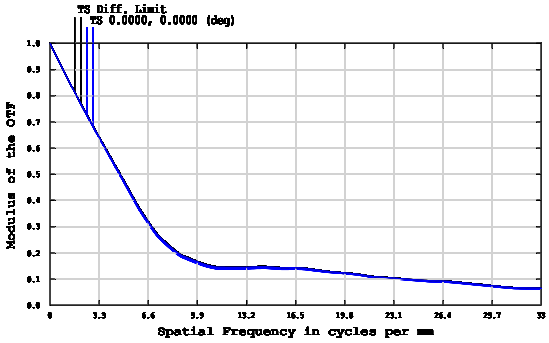

Figure 14: Monte Carlo Analysis On-Axis MWIR MTF

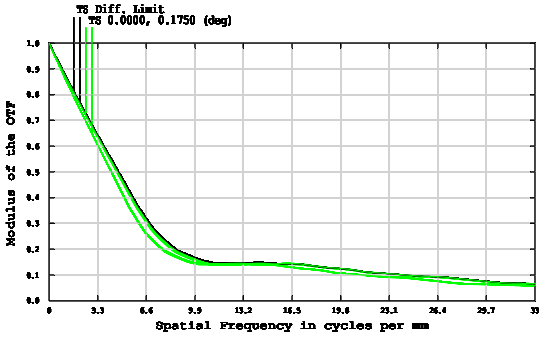

Figure 15: Monte Carlo Analysis 0.175° Field MWIR MTF

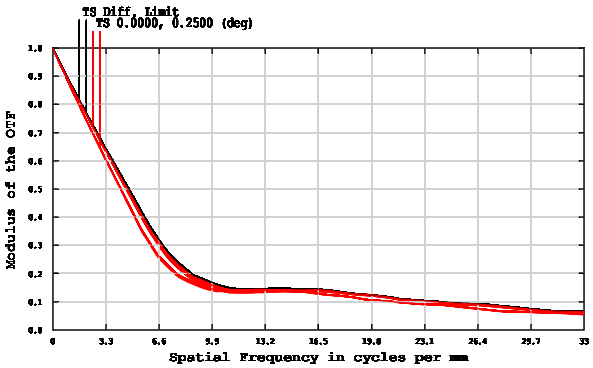

Figure 16: Monte Carlo Analysis 0.25° Field MWIR MTF

The MTF degradation in the MWIR is negligible due to the simulated elevation and azimuth errors and the system performance may be considered diffraction limited.

CURRENT AND FUTURE RESEARCH

Four Segment Deployable Primary Mirror

SDL is currently working on aligning and testing a deployable four petal parabolic primary mirror based on the single petal hardware described in this paper. Figure 17 and Figure 18 show the hardware in the stowed and deployed configurations with four petals. All four petals have demonstrated sub-arcsecond standard deviation repeatability similar to the single petal hardware. Plans are in place to test the primary for interferometric wavefront error repeatability. This test will use an interferometer to measure the wavefront error after successive stow and deploy sequences of all four petals simultaneously. Wavefront error repeatability will show how well all four petals stay in alignment throughout a deployment cycle.

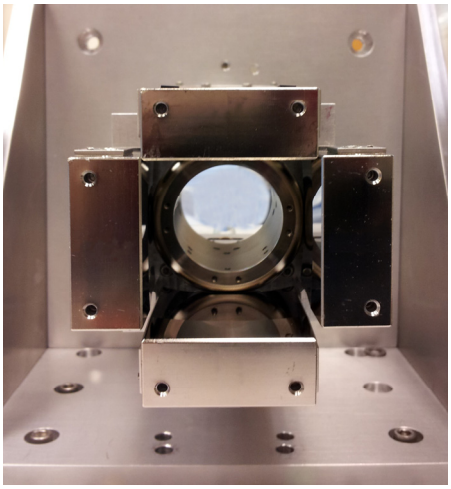

Figure 17: Stowed Four Petal Primary Mirror

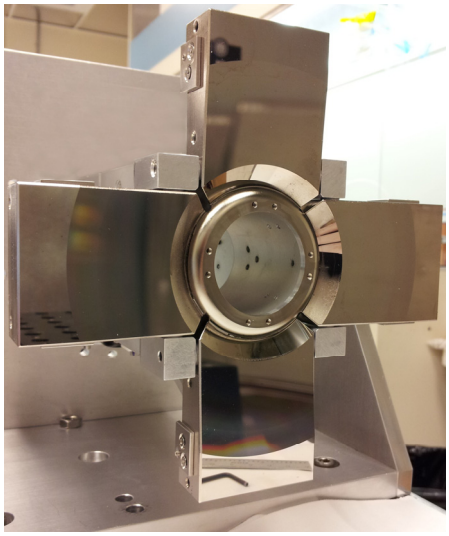

Figure 18: Deployed Four Petal Primary Mirror

Deployable Secondary Mirror

The current F/7 Cassegrain optical design requires a secondary-to-focal plane distance of 275 mm. Reserving approximately 50 mm of payload length for a focal plane array and electronics, the total camera payload length required would be 325 mm. This length can be dramatically reduced with the implementation of a deployable secondary mirror. Deployment of the secondary mirror will provide for a reduced stowed telescope launch volume. Current estimates predict that the telescope payload length could be reduced 150 mm to 175mm, nearly a 50% reduction.

The optical model alignment sensitivity analysis was also applied to the secondary mirror deployment. The secondary mirror deployed positioning requirement is much less stringent than what is required for the primary mirror. Recalling the results from the petal alignment sensitivity, the misaligned petals are expected to contribute 88 nm RMS of wavefront error to the system. The secondary mirror can have a decenter alignment error (translation in the optical XY plane) of nearly 0.30 mm and a tip/tilt error of 0.19 degrees (684 arcseconds) before its contributions to the system wavefront error approach that of the four petal angular misalignments. Figure 19 and Figure 20 give the secondary mirror sensitivity to de-centration and tip/tilt errors.

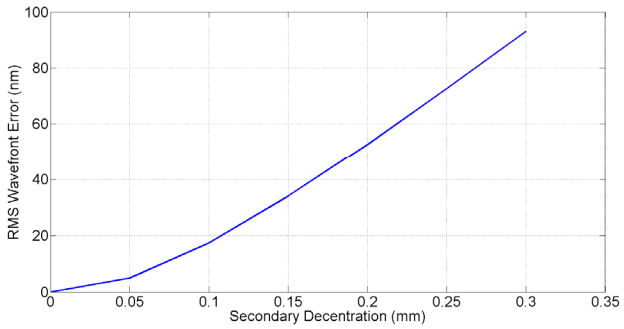

Figure 19: WFE vs. Secondary Decenter Error

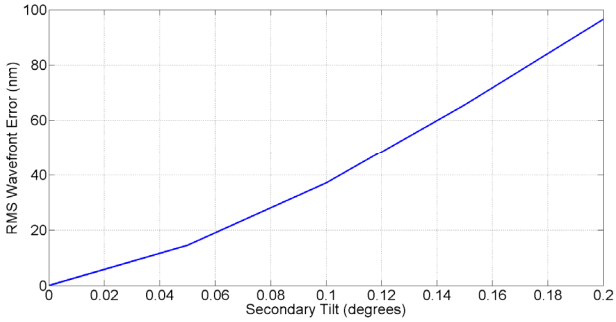

Figure 20: WFE vs. Secondary Tip/Tilt Error

Lastly despace or primary-to-secondary mirror separation error along the optical Z axis direction is much more sensitive to the system wavefront error. Figure 21 shows that only 0.016 mm of despace error will produce the equivalent RMS wavefront error as that of the misaligned petals. A re-focus adjustment could drastically reduce the system sensitivity to despace error. These initial sensitivity results show us that the secondary mirror deployment should not drive the full optical system performance.

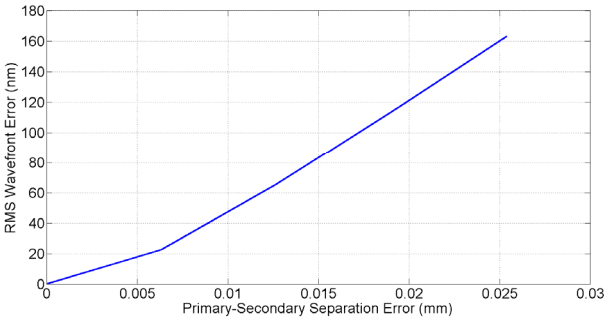

Figure 21: WFE vs. Primary-to-Secondary Separation Error

The deployable secondary mirror is currently in a design and construction phase. It will first be built and tested independent of the primary mirror. After a successful build and test effort, it will be integrated with the deployable primary mirror. Figure 22 and Figure 23 show the current integrated concept design of a stowed and deployed secondary/primary mirror respectively.

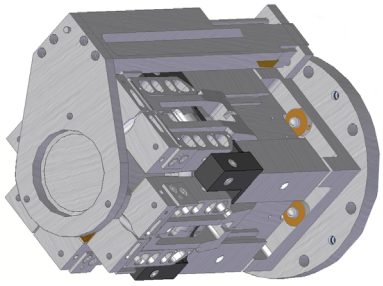

Figure 22: Deployable Secondary and Primary Stowed

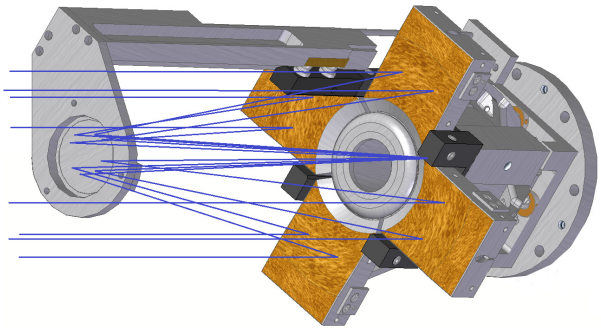

Figure 23: Deployable Secondary and Primary Deployed

Technology Readiness Level (TRL)

NASA has established a set of Technology Readiness Levels helping prepare new technologies for successful flight operation.[5] SDL is working to mature the DPT to a level of space flight readiness or TRL 6. At TRL 6, a near final system has been demonstrated in the relevant flight environments. With the successful single petal and multiple petal demonstrations, DPT is considered to be at a TRL 4. At TRL 4, a basic prototype or example of the technology are demonstrated in a laboratory environment. In the next year, plans are in place to integrate the four petal primary mirror with a deployable secondary mirror and a focal plane array at the telescope focus. Combining an aligned telescope with a sensor completes a DPT imaging system. This system will then be used to capture imagery and verify image quality models. Environmental effects of vibration and temperature cycling can also be explored. More realistic demonstrations and tests such as these will increase the readiness level to TRL 5.

CONCLUSION

The single deployable petal proof of concept test measured the elevation and azimuth angular alignment standard deviation errors to be less than 0.6 arcseconds in each axis. Using alignment sensitivities and Monte Carlo simulations within ZEMAX optical design software, SDL determined that these errors would allow excellent image quality in the SWIR and longer wavelengths for a four petal Cassegrain imaging system. Image quality degradation starts to become evident in the low end of the SWIR and aberrations due to petal angular alignment errors dominate in the near-infrared and visible spectrums. Even though imagery within these spectrums will not be diffraction limited, image quality will be acceptable for non-imaging applications such as LiDAR and laser communications. SDL will continue to research a deployable four petal primary mirror to measure the wavefront error repeatability interferometrically. Plans are also in place to incorporate a deployable secondary mirror to the DPT as well as a focal plane array in the next year. At this point it will be possible to obtain imagery and verify image quality models. The DPT is currently estimated to be at a NASA TRL 4 and should be at TRL 5 within a year.

Acknowledgments

The SDL DPT team would like to thank the Utah State University Research Foundation for providing generous funding for this research.

References

1. Gaskill, J.D., Linear Systems, Fourier transforms, and Optics, John Wiley and Sons, New York, 1978.
2. Dereniak, E.L. and Boreman, G.D., Infrared Detectors and Systems, John Wiley and Sons, New York, 1996.
3. "The telescope that ate astronomy". Nature. 27 October 2010.
4. Smith, W.J., Modern Optical Engineering, The Design of Optical Systems, Second Edition, McGraw Hill, New York, 1990.
5. Mankins, J., "Technology Readiness Levels," NASA, Office of Space Access and Technology, Advanced Concepts Office, Apr., 1995. http://www.hq.nasa.gov/office/codeq/trl/trl.pdf